PNAS RESEARCH ARTICLE | EVOLUTION

Extreme elevational migration spurred cryptic speciation in giant hummingbirds

Jessie L. Williamson[a,b,c,d,1], Ethan F. Gyllenhaal[a,b], Selina M. Bauernfeind[a], Emil Bautista[e], Matthew J. Baumann[a], Chauncey R. Gadek[a,b,f], Peter P. Marra[g], Natalia Ricote[h], Thomas Valqui[e,i], Francisco Bozinovic[j], Nadia D. Singh[k], and Christopher C. Witt[a,b,1]

Edited by Scott Edwards, Harvard University, Cambridge, MA; received August 11, 2023; accepted March 19, 2024

The ecoevolutionary drivers of species niche expansion or contraction are critical for biodiversity but challenging to infer. Niche expansion may be promoted by local adaptation or constrained by physiological performance trade-offs. For birds, evolutionary shifts in migratory behavior permit the broadening of the climatic niche by expansion into varied, seasonal environments. Broader niches can be short-lived if diversifying selection and geography promote speciation and niche subdivision across climatic gradients. To illuminate niche breadth dynamics, we can ask how "outlier" species defy constraints. Of the 363 hummingbird species, the giant hummingbird (*Patagona gigas*) has the broadest climatic niche by a large margin. To test the roles of migratory behavior, performance trade-offs, and genetic structure in maintaining its exceptional niche breadth, we studied its movements, respiratory traits, and population genomics. Satellite and light-level geolocator tracks revealed an >8,300-km loop migration over the Central Andean Plateau. This migration included a 3-wk, ~4,100-m ascent punctuated by upward bursts and pauses, resembling the acclimatization routines of human mountain climbers, and accompanied by surging blood-hemoglobin concentrations. Extreme migration was accompanied by deep genomic divergence from high-elevation resident populations, with decisive postzygotic barriers to gene flow. The two forms occur side-by-side but differ almost imperceptibly in size, plumage, and respiratory traits. The high-elevation resident taxon is the world's largest hummingbird, a previously undiscovered species that we describe and name here. The giant hummingbirds demonstrate evolutionary limits on niche breadth: when the ancestral niche expanded due to evolution (or loss) of an extreme migratory behavior, speciation followed.

cryptic speciation | elevational migration | high-altitude biology | hummingbirds | population genomics

Significance

Biodiversity varies from place to place because the range of climates suitable for any one species tends to be limited. The giant hummingbird appears to defy this tendency, occurring across the broadest range of environments of any hummingbird. We asked whether its migration, physiology, or genetics explain its climate generalism, potentially illuminating mechanisms of niche breadth evolution. Microtracking devices revealed an epic migration from the Chilean coast to the Peruvian Andes, with an extreme, >4,100-m elevational shift and corresponding performance trade-offs. Genomes revealed that migrant and resident populations diverged in the Pliocene and have since evolved under phenotypic stasis. A migratory shift enabled climatic niche expansion, leading to speciation and niche subdivision, consistent with diversification by niche breadth oscillation.

A key to the maintenance of biodiversity is that the climatic breadth of a species niche is intrinsically constrained against continual expansion. Constraints on species niche breadth are thought to be caused by traits with environment-specific performance trade-offs and limited potential for local adaptation (1–3), but our understanding of these constraints remains a major challenge for evolutionary ecology (4–6). Across the 363-species radiation of hummingbirds, breeding ranges exhibit strikingly limited climatic niche breadth: 90% of species span <22° of latitude and <2,000 m of elevation (*SI Appendix*, Fig. S1), despite relatively few species having physical barriers to niche expansion (7). One reason for the dearth of species with broad niches could be a tendency for generalist species to diversify into more specialized descendant species (8). Repeated expansion and contraction of niche breadth have been hypothesized to drive diversification by the cyclic subdivision of the climatic and geographic space occupied by generalist species (e.g., refs. 9–11). Such oscillations could be difficult to detect using comparative methods (12, 13), but their occurrence would suggest that drivers of niche breadth expansion also promote speciation along axes of niche variation. For vagile species such as birds, shifts in migratory behavior are one mechanism by which breeding ranges can expand into varied environments (14–16), broadening the climatic niche. As expected under this mechanism, migratory hummingbird species tend to breed across broader latitudinal and elevational ranges than sedentary ones (*SI Appendix*, Fig. S1). In this way, niche breadth expansion that occurs when migratory behaviors diversify can help explain why shifts in migratory behavior tend to be associated with accelerated diversification (e.g., ref. 17).

One path to understanding constraints on niche breadth is to test why certain species defy those constraints. In hummingbirds, there is one outlier species whose breeding range has exceptional elevational and latitudinal breadth: the giant hummingbird (*Patagona gigas*, Gray 1840; *SI Appendix*, Fig. S1). This species breeds across 39° of latitude and >4,400 m of elevation, but this is not the only way in which the giant hummingbird seems to bend the rules of life. It is the most phylogenetically distinct

Author contributions: J.L.W. and C.C.W. designed research; J.L.W., E.F.G., S.M.B., E.B., M.J.B., C.R.G., N.R., and C.C.W. performed research; J.L.W. analyzed migration, blood, and morphological data; J.L.W. and E.F.G. analyzed genomic data; J.L.W. contributed tables and figures; J.L.W., P.P.M., T.V., F.B., N.D.S., and C.C.W. provided critical resources; and J.L.W. and C.C.W. wrote the paper with input from all authors.

The authors declare no competing interest.

This article is a PNAS Direct Submission.

[1]To whom correspondence may be addressed. Email: jlw432@cornell.edu or cwitt@unm.edu.

This article contains supporting information online at https://www.pnas.org/lookup/suppl/doi:10.1073/pnas.2313599121/-/DCSupplemental.

Published May 13, 2024.

hummingbird, having evolved on its own branch for ~14 Mya (18). It evolved massive size (17 to 31 g), approximately twice as large as the next largest hummingbird, rendering its hovering, nectivorous lifestyle biomechanically and energetically improbable (19, 20). At tropical latitudes, giant hummingbirds reside year-round in the high Andes; however, southern temperate populations breed at sea level and embark on a mysterious migration during the austral winter. In 1834, Charles Darwin witnessed their spring arrival from the "parched deserts of the north" (21), a reference to the Atacama Desert of northern Chile. Ornithologists have since hypothesized that the nonbreeding range might include the Andes of southeastern Bolivia or northwestern Argentina (e.g., ref. 22), but the migratory journey and nonbreeding range have remained unknown, in part due to the technical challenges of tracking lightweight species (23).

In this study, we sought to test how the giant hummingbird is apparently able to maintain such an extraordinarily broad environmental niche. To elucidate the role of migration in niche breadth expansion, we used satellite transmitters and geolocators to track giant hummingbirds from sea-level breeding areas in Chile. To test for evidence of performance trade-offs, we collected respiratory trait data from >175 individuals across the elevational range. To test for local adaptation and/or lineage divergence, we analyzed genomic sequences from 101 individuals across the geographic range. The results revealed an extraordinary loop migration across the Central Andean Plateau, up to >8,335 km, and accompanied by shifts of >4,100 m in elevation. A decisive divergence event in the late Pliocene sundered the giant hummingbird into extreme elevational migrant and high-elevation resident species, reproductively isolated and differentially adapted, but with external phenotypes evolving under stasis. The giant hummingbirds remain anomalous in several ways, but with respect to constraints on niche breadth, they are an exception that proves a rule: Niche breadth expansion via a shift in migratory behavior led to speciation with niche subdivision.

Results and Discussion

Extreme Latitudinal and Elevational Migration. We uncovered migration routes and locations of nonbreeding areas from eight giant hummingbirds tracked with geolocators or satellite transmitters (Fig. 1*A*) (23). Chilean giant hummingbirds initiated autumn migration in mid-February to early March, traveling 5,457 to 8,335 km roundtrip ($\bar{x}$ = 6,578 km). Their circular route followed the Andes to the north, passing through the breeding ranges of populations in Argentina, Bolivia, and Peru. Individuals arrived at nonbreeding areas in southern and central Peru in early May to July, ~90 to 150 d after beginning migration (Fig. 1 *A* and *B*). The ~30-d southbound spring return to Chile typically followed the western slope of the Andes, crossing the Atacama Desert (Fig. 1*A*). The giant's journey is one of the longest hummingbird migrations in the world, overlapping in distance with that of the rufous hummingbird (*Selasphorus rufus*), which flies up to ~8,200 km roundtrip annually (24).

Each migrant giant hummingbird spent time at multiple nonbreeding sites (*SI Appendix*, Table S1). Hummingbirds spent 4 to 77 d, varying by individual, around Cusco Department, Peru (ca. 14° S to 13° S), before reaching their northernmost nonbreeding

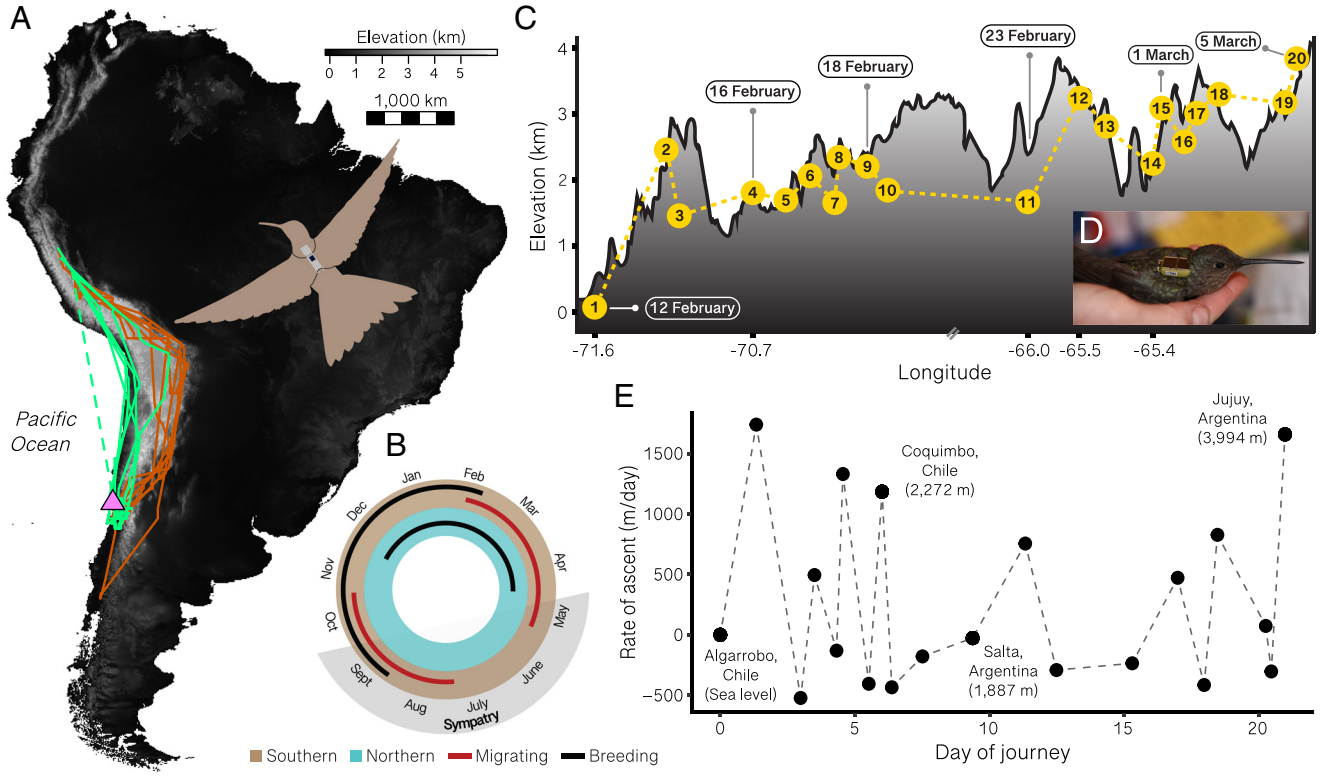

Fig. 1. Extreme latitudinal and elevational migratory journey. (*A*) Migration routes for seven geolocator-tracked southern giant hummingbirds showing the 5,457 to 8,335 km roundtrip journey from sea-level breeding grounds in Algarrobo, Chile (pink triangle) to high elevation nonbreeding areas in central Peru. Orange lines depict northerly (autumn) migration, green lines depict southerly (spring) migration; dashed line indicates inferred trajectory. Giant hummingbird with geolocator backpack illustration from ref. 23. (*B*) Seasonal phenology chronogram of giant hummingbirds showing species range overlap from May to September. (*C*) Elevational ascent of a giant hummingbird, illustrated by high-resolution Argos satellite tracking data from PTT177846. Over 21 d, bursts of ascent were interspersed with pauses and even slight downward movements. The bird stopped at mid-elevations to acclimatize before ascending the high peaks of the Andes. (*D*) Giant hummingbird with a satellite transmitter, photo by Chris Witt. (*E*) Rates of elevational ascent during the northward migratory journey from satellite tracks. Each point indicates the rate of ascent between two satellite readings.

areas at 9.0° S to 11.7° S, where they spent 30 to 109 d. The annual migratory loop appeared to be synchronized with floral nectar resources: Southbound spring migration coincided with the flowering of columnar cacti on the west slope of the Andes, such as *Weberbauerocereus weberbaueri* (25); and flowering for several cactus species in central Chile, including *Echinops litoralis* and *Eriocyse subgibbosa*, peaks during the giant hummingbird breeding season (26–28).

Our tracking data showed that southern giant hummingbirds are one of the ~100 bird taxa that undertake 'elevational niche-shift migration', fluctuating ≥2,000 m and acclimatizing to drastically different atmospheric pressures biannually (29). During migration, the satellite-tracked giant hummingbird shifted in elevation by at least ~4,160 m (Fig. 1 *C* and *E* and *SI Appendix*, Fig. S3 and Table S1). From sea level, it displayed an upward burst, followed by an 8-d pause at ~1,640 to 2,270 m, followed by a second burst and a 9-d pause at ~2,290 to 3,215 m, before a final push to elevations >3,995 m (Fig. 1 *C* and *E*). The bird crossed from Coquimbo, Chile, over the Andes, and into Catamarca, Argentina during a ~45-h period between 19 and 21 February 2019 (Fig. 1*C*), traveling 685 km at an average rate of 15.3 km/h, including stops.

The burst–pause tempo of ascent during the first 21 d of the giant hummingbird's journey (Fig. 1 *C* and *E*) resembled the tempo of human mountaineers, who intersperse protracted acclimatization periods at elevationally stratified camps with carefully timed upward climbs (30, 31). Exercise studies have demonstrated that residence at 2,200 m or higher for 1 to 2 d induces ventilatory acclimatization, and that 6 d acclimatization at 2,200 m substantially increases hypoxia tolerance at 4,300 m and reduces incidence and severity of altitude sickness during subsequent rapid ascent (32). We posit that the giant's three upward bursts and two multiday, mid-elevation rest periods likely comprise a behavioral strategy that provides time for acclimatization to progress, reducing risk of harm from acute altitude exposure (e.g., refs. 30 and 31).

Cryptic Divergence Across a Migratory Divide. We sequenced whole genomes of 36 individuals and regions flanking ultraconserved elements (UCEs) of 65 individuals from sedentary northern and migratory southern populations across the species range (*SI Appendix*). We analyzed three different datasets: 1) 100,238 of >43 million single nucleotide polymorphisms (SNPs) from whole genomes ($\bar{x}$ coverage = 16.6×; range = 9.11 to 27.8×; 75% complete); 2) 4,126 SNPs from a subset of UCEs from tissue (n = 35 birds; 100% complete); and 3) 4,416 SNPs from a combined UCE dataset with n = 70 individuals (90% complete).

We identified two reproductively isolated and distinct biological species that do not correspond to current subspecies designations: a northern, nonmigratory species ranging from southern Colombia to at least southern Peru; and a southern, migratory species ranging seasonally from central Chile to central Peru (Fig. 2*A* and *SI Appendix*, Fig. S4). The two species diverged between 2.1 and 3.4 Mya (Fig. 2 *B–F* and *SI Appendix*, Fig. S5). Population assignment analyses favored these same two gene pools (K = 2) and revealed within-species population structure along a latitudinal gradient (Fig. 2*D*). Mitochondrial haplotype networks corroborated nuclear genomic results (Fig. 2*E*). Mean genome-wide F_{ST} between the lineages was 0.61 (Fig. 2*H*), consistent with a long period of isolation. We detected little to no gene flow in any part of the species' ranges (*SI Appendix*, Table S2), although ABBA/BABA tests suggested possible low levels of past introgression between populations from Ecuador and Chile, Ecuador and Argentina, and Chile and Peru, respectively (*SI Appendix*, Table S2).

We identified one northern × southern hybrid, a male collected in west-central Peru during spring (Fig. 2 *B* and *C* and *SI Appendix*). The hybrid, an F1 between Peruvian and Argentinian parents (H_O = 0.446, F = –0.912 and *SI Appendix*, Fig. S6), had a genomic population assignment intermediate between northern and southern forms (Fig. 2*A*), a northern mitochondrial haplotype (Fig. 2*E*), and an indeterminate phenotype (*SI Appendix*, Fig. S6). The occurrence of a hybrid out of 101 sampled individuals suggests breeding range overlap and regular hybridization (Fig. 2 *B* and *C*). Under a binomial distribution with α = 0.05, our observed proportion of hybrids (0.01) was compatible with a range of possible true proportions in the wild population (0.0005 to 0.046). In light of our effective population size (N_e) estimates (~65,000 in Peru), this frequency of hybrids would imply at least dozens of hybridization events per generation. However, the high genome-wide F_{ST} between the two species (0.61) is consistent with no more than one introgressive hybrid every six generations (35), and dearth of backcrossed hybrids suggests that no gene flow is occurring. The data are therefore most consistent with hybrid unfitness and postzygotic reproductive isolation (36, 37). One caveat is that the extent and timing of gene flow after initial divergence remains uncertain, as evidenced by the small, recent admixture proportion between populations of northern and southern giant hummingbirds (*SI Appendix*, Table S2) and close matching of N_e as recently as 180 ka (Fig. 2*G*).

A single evolutionary shift in migratory behavior likely occurred in conjunction with giant hummingbird speciation. This shift could have been either a loss (i.e., migratory drop-off) or gain of migration. Gains of migration clearly occur during bird evolution (e.g., ref. 38), but losses of migration are more frequently implicated in speciation (14, 15, 17, 39, 40) and occur regularly and rapidly enough to have been observed during historical time (16, 41). Although it is not possible to know the direction of the giant hummingbird migratory shift with certainty, geologic and genomic evidence provide clues about the migratory behavior of the most recent common ancestor. The Central Andean Plateau was ~1/2 its current elevation before rapid uplift occurred that would have expanded giant hummingbird habitat at low latitudes in the late Miocene–Pliocene (42), immediately preceding speciation. This geologic history suggests shifts in available habitat in the Central Andes that could have been associated with migratory drop-off or potentially range expansion leading to gain of migration (43). We used genome sequences to test for signatures of reduced N_e in the northern species that would be expected to follow a migratory drop-off event, while recognizing that estimates of N_e over geologic time are prone to imprecision (Fig. 2*G*). Both species exhibited long-term N_e stability, with Tajima's D values near zero and relatively uniform nucleotide diversity across populations but marginally lower diversity at range edges and in the northern species (*SI Appendix*, Table S4). Since the late Pleistocene, ~180 ka, N_e estimates of northern populations remained constant or decreased, while those of southern populations increased; prior to this period, northern and southern populations had roughly equal N_e (Fig. 2*G*). By the LGM (~22,000 ka.), N_e estimates for the sedentary northern species were ~1/2 those of the migratory southern species (Ecuador N_e = 28,000; Peru N_e = 65,000; Chile N_e = 118,000; Argentina N_e = 156,000; Fig. 2*G*).

Cryptic but Not Identical Phenotypes. We analyzed measurements of 361 giant hummingbirds to describe differences in external phenotype between the two species. Northern giant hummingbirds were larger, on average, with longer bills ($P = 2.2 \times 10^{-16}$), wings ($P = 1.31 \times 10^{-9}$), tails ($P = 1.4 \times 10^{-2}$), and tarsi ($P = 7 \times 10^{-4}$; Fig. 3 and *SI Appendix*, Table S4) than southern giant hummingbirds. Males of both species were heavier and longer-winged than females (*SI Appendix*, Fig. S7). Most individuals were

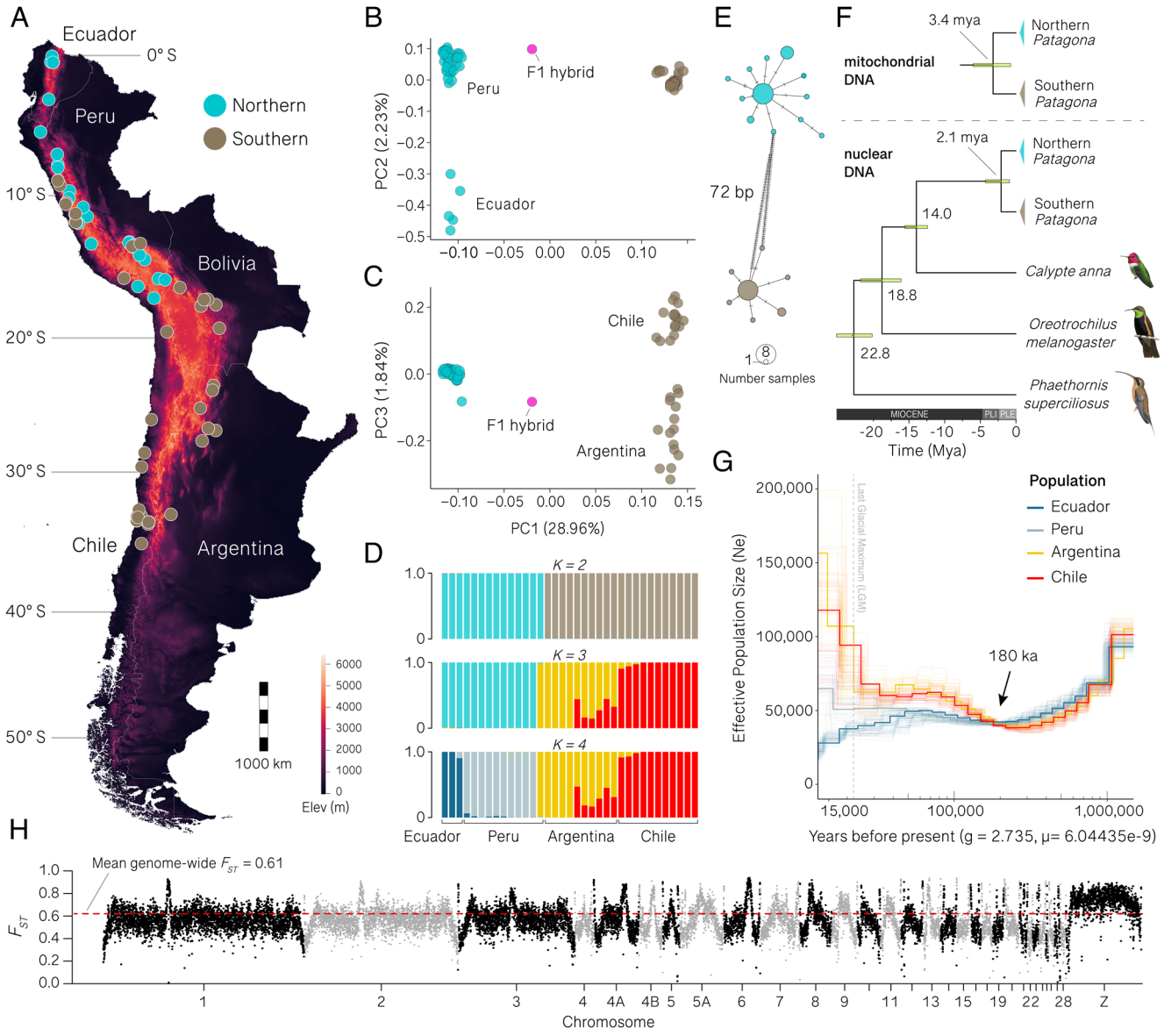

Fig. 2. Population structure and landscape of divergence in giant hummingbirds. (*A*) Giant hummingbirds inhabit distinct latitudinal and elevational ranges and co-occur seasonally in the central Andes (n = 361 individuals). (*B* and *C*) PCA (4,416 SNPs from UCEs of n = 70 individuals) illustrates strong species differentiation and structure within each northern and southern species. (*D*) sNMF analysis of 35 whole genomes showing K = 2 (best fit), K = 3, and K = 4 scenarios confirms that no admixed individuals were detected between northern and southern species. Country labels denote sampling origin; colors correspond to ancestry; color key in *G*. (*E*) *ND2* haplotype network (n = 63 individuals) illustrates strong between-species mitochondrial divides. (*F*) Time-calibrated maximum clade credibility trees estimate divergence of northern and southern giant hummingbirds 2.1 to 3.4 Mya (nuclear DNA 95% HPD: 0.9 to 4.3 Mya; mitochondrial DNA 95% HPD 2.1 to 4.7 Mya). Horizontal lime green bars denote 95% highest probability density estimates. Hummingbird illustrations courtesy (33). (*G*) Pairwise sequentially Markovian coalescent (PSMC) showing historical divergence in effective population size (N_e) between the two species ~180 ka. Spiderweb trace shows 50 bootstrap replicates for each sample. Last glacial maximum (LGM) (22,000 ka). Reliability of N_e estimates is known to diminish closer to the present (34). (*H*) Genome-wide genetic differentiation between northern and southern giant hummingbirds, shown in 50 kb windows; red line at mean genome-wide F_{ST}.

phenotypically distinguishable, despite crypsis sufficient to have hidden species co-occurrence for nearly two centuries (Fig. 3); however, substantial overlap existed between species and sexes, respectively (Fig. 3 and *SI Appendix*, Fig. S9). Linear discriminant analyses for each sex correctly identified ~80% of individuals. Key features such as throat color and pattern appear paramount for field identification (Fig. 4*E* and *SI Appendix*, Fig. S11).

The shorter wing length of the long-distance migrant southern giant hummingbird (by 5.6 mm, on average; Fig. 3 and *SI Appendix*, Table S4) seems paradoxical because of the evolutionary tendency for longer wings in migratory birds and at high latitudes (e.g., refs. 44 and 45). However, hummingbird wing length increases with altitude to generate lift in thin air (46); therefore, data suggest that wing length in giant hummingbirds may have evolved for competitive performance at breeding elevations, rather than for flight efficiency during long-distance migration (*SI Appendix*).

Hemoglobin Adaptation and Hypoxia-Induced Blood Plasticity. Hypoxia at high elevation is a strong selective pressure that can lead to rapid and predictable genetic adaptation (e.g., refs. 47–49). At shorter timescales, large-scale shifts in elevation between the breeding and nonbreeding grounds are impactful for respiratory physiology, requiring compensatory physiological responses. We analyzed hemoglobin (Hb) genotypes, blood traits related to O_2-carrying capacity (50), and heart and lung sizes to test for evolved and plastic differences between the two giant hummingbird species. We predicted that differences between southern elevational migrants at low and high elevations would reveal the extent of

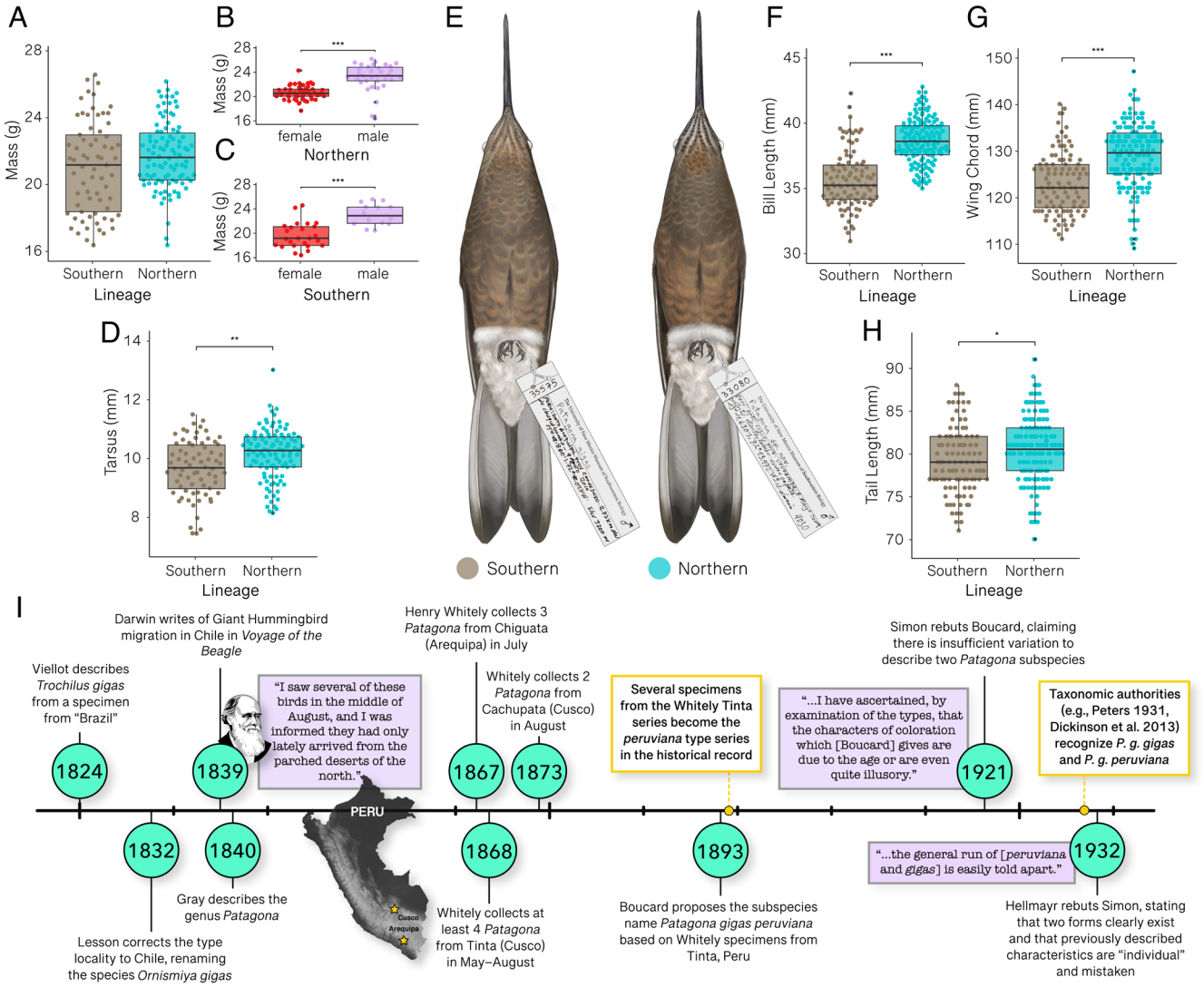

Fig. 3. Cryptic but distinguishable plumage and morphology add to historical uncertainty surrounding giant hummingbird evolution. (*A–C*) Northern (n = 162) and southern (n = 116) giant hummingbirds do not differ in mass, but males of each species are significantly heavier than females (both $P < 6.89 \times 10^{-6}$, t test or Wilcoxon rank-sum test). On average, male northern giant hummingbirds are 2.5 g heavier and male southern giant hummingbirds are 3.4 g heavier than their respective females. (*D*) Northern giant hummingbirds have significantly longer tarsi than southern giant hummingbirds. (*E*) Comparison of diagnostic plumage features of northern and southern giant hummingbirds, illustrated from Museum of Southwestern Biology (MSB) specimens (southern: MSB:Bird:35575; northern: MSB:Bird:33080). Illustrations by Jillian Ditner, Cornell Lab of Ornithology. (*F-H*) Northern giant hummingbirds have significantly longer bills, wings, and tails than southern giant hummingbirds (all external measurements $P < 1.4 \times 10^{-2}$; all t test or Wilcoxon rank-sum test). Sample sizes vary by trait analyzed (*SI Appendix*). Box plot horizontal lines indicate median values. Each point is a value from a single individual. (*I*) Timeline of key dates and events in the *Patagona* historical record, which has remained contentious since the mid-1800s. See *SI Appendix*, Table S5 for additional details about possible type specimens.

seasonal phenotypic flexibility in response to extreme elevational shifts (29). Similarly, any differences between northern high-elevation residents and southern elevational migrants at high elevations would distinguish the evolutionary responses to permanent versus intermittent hypoxia challenges, potentially revealing performance trade-offs in the elevational migrants.

We sequenced the Hb β^A-globin subunit from 25 southern individuals and found that both species share high-altitude-adapted Hb with identical amino acids at positions Hb β^A-13 and Hb β^A-83 (Fig. 4*a*). Hb β^A-13_{SER} has evolved independently in at least three other hummingbird genera (*Chalcostigma*, *Pterophanes*, and *Oreotrochilus*) that occur at extreme high altitudes (29, 47). Thus, an extreme elevational migrant species appears to be fixed for a β^A-globin genotype that is otherwise exclusive to hummingbird species occurring at the highest elevations, suggesting that the southern giant hummingbird has a genetic mismatch with its environment during its low-elevation breeding season.

From 2006 to 2022, we collected blood, lung, and heart data from 175 individual giant hummingbirds from three populations: southern elevational migrants at sea level in Chile, southern elevational migrants at high elevation (2,908 to 4,082 m) in Peru, and northern high-elevation residents in Peru (Fig. 4*B*). We measured six blood traits known to affect O_2-carrying functions: total hemoglobin concentration ([Hb]), hematocrit (Hct), total red blood cell count (TRBC), MCV, mean cellular hemoglobin content (MCH), and mean cellular hemoglobin concentration (MCHC) (50).

Southern giant hummingbirds exhibited striking seasonal flexibility. At high elevations, migrants had elevated [Hb] ($P < 1 \times 10^{-5}$), Hct ($P < 1 \times 10^{-4}$), and MCH ($P = 4.9 \times 10^{-2}$; all Dunn or Tukey's post hoc tests; Fig. 4). Between the low-elevation breeding grounds and high-elevation nonbreeding grounds, migrants increased [Hb] by 2.7 g/dL, Hct by 7.1%, and MCH by 9.4 pg, on average (Fig. 4). Like human mountaineers, they acclimatized to high elevations by increasing [Hb] and Hct during ascent,

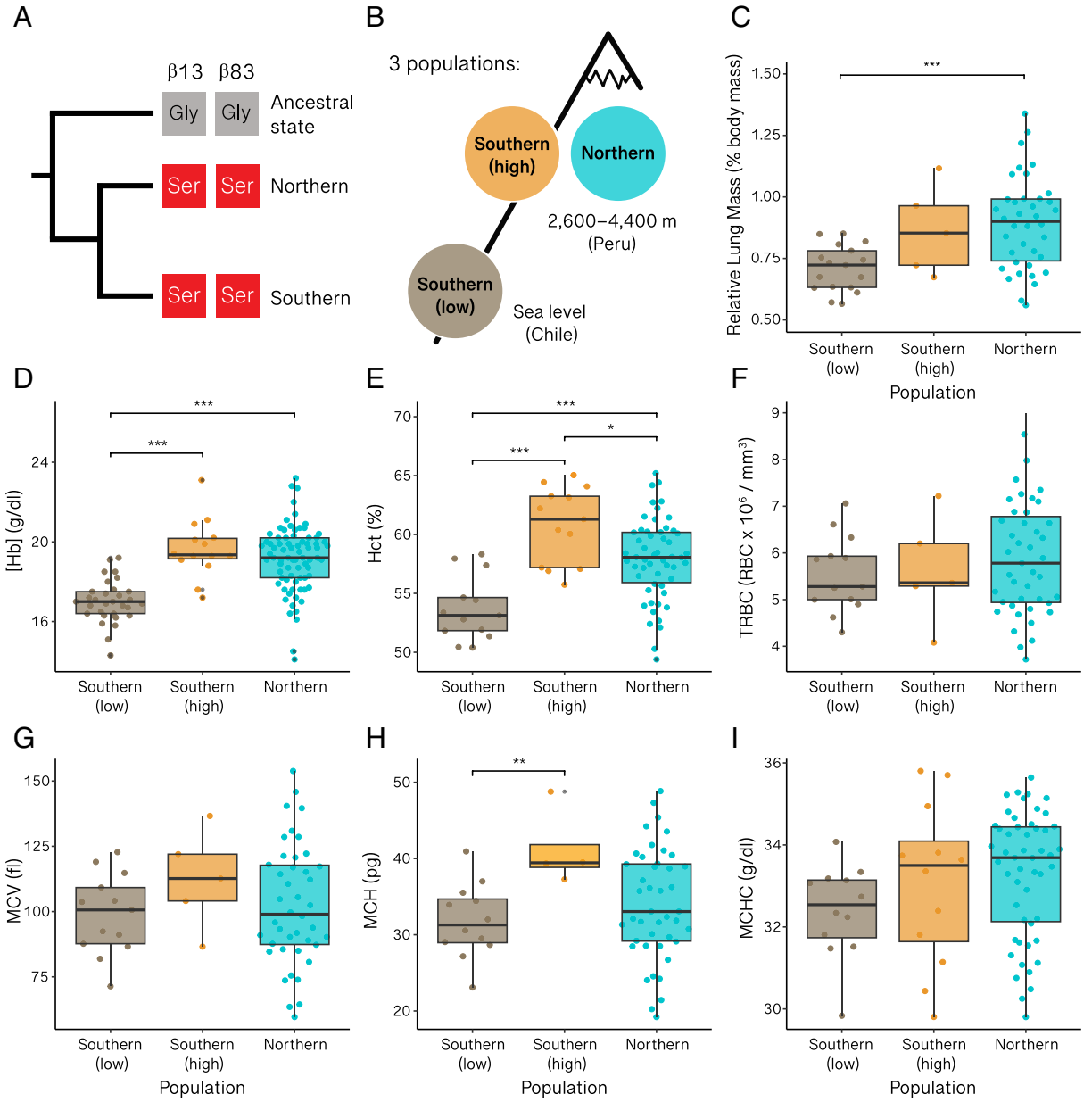

Fig. 4. Hemoglobin genetic adaptations and physiological differences among populations of low- and high-elevation giant hummingbirds. (*A*) Northern and southern giant hummingbirds share hemoglobin genetic adaptations. (*B*) Field sampling of three populations across elevations. (*C*) Northern high-elevation residents had significantly greater lung masses (23% larger, on average) than southern elevational migrants at low elevation ($P = 0.002$, Kruskal–Wallis test with Dunn post hoc test). (*D* and *E*) Hemoglobin concentration ([Hb]) and Hematocrit (Hct) were significantly elevated in southern elevational migrants at high versus low elevation ([Hb]: $P < 1 \times 10^{-5}$, Dunn post hoc test; Hct: $P < 1 \times 10^{-4}$, Tukey's post hoc test). [Hb] and Hct were also significantly elevated in northern high-elevation residents compared to southern elevational migrants at low elevation ([Hb]: $P < 1 \times ^{-5}$, Dunn post hoc test; Hct: $P < 3 \times ^{-4}$, Tukey's post hoc test). Hct was significantly higher in southern elevational migrants at high elevation than in northern high-elevation residents ($P = 1.5 \times ^{-2}$, Tukey's post hoc test). (*F*) Total red blood cell count (TRBC) and (*G*) mean cell volume (MCV) did not differ among populations. (*H*) Mean cell hemoglobin (MCH) was significantly elevated in southern elevational migrants at high versus low elevation ($P = 4.9 \times ^{-2}$, Tukey's post hoc test). (*I*) Mean cell hemoglobin concentration (MCHC) did not differ among any populations. Sample sizes vary by trait analyzed (*SI Appendix*). See additional details in *SI Appendix*, Table S7. Box plot horizontal lines represent median values. Each point is a value from a single individual.

approaching the blood phenotype of high-elevation residents (Fig. 4 *D* and *E*). In a study of North American songbirds and hummingbirds, Carey and Morton found that elevational migrants at high elevations did not differ in blood traits from elevational residents (51). Similarly, we found no differences between southern elevational migrants at high elevations and northern high-elevation residents in [Hb], TRBC, MCV, MCH, or MCHC (all $P > 0.11$, One-way ANOVA or Kruskal–Wallis test; Fig. 4 *D*, *F*, and *I*). However, Hct was significantly higher in southern elevational migrants at high elevation than in northern high-elevation residents ($P = 1.5 \times 10^{-3}$, Tukey's post hoc test). This suggests "overcompensation" by elevational migrants during their temporary residency at high elevations, providing a potential basis for performance deficit, or trade-off. Analogous overproduction of red blood cells in response to low partial pressure of O_2 occurs in some human populations, with harmful side effects (52).

Lung mass was strongly linked to natal elevation (Fig. 4*C*), though neither flight muscle masses nor heart masses were different between the two species (*SI Appendix*, Fig. S12). After correcting for body size, the high-elevation resident species had greater lung masses, ~23% larger than elevational migrants at low elevations ($P = 1.1 \times 10^{-3}$, Kruskal–Wallis with Dunn post hoc test). This finding is reminiscent of Andean humans who have evolved larger pulmonary volumes than humans of lowland

ancestry, but in whom lung size can vary by 15 to 42% depending on natal altitude (53). In both humans and giant hummingbirds, greater pulmonary volume increases diffusion capacity via greater surface area for gas exchange (53).

The World's Largest Hummingbird Is Undescribed. In 1824, *P. gigas* was described from a single southern-form specimen from Chile (54). A dubious subspecies, *P. g. peruviana*, was subsequently named from two to three specimens (syntypes) collected from southern Peru (Fig. 3*I* and *SI Appendix*, Table S5) (22, 55). The plumage characteristics that formed the basis for its description later proved to be indicators of age and plumage wear, not taxonomic identity (22, 55, 56). Further increasing confusion, the type specimens used to name *peruviana*, all collected by Henry Whitely, were from the May to August nonbreeding months when northern and southern lineages occur together in Peru.

We sequenced UCEs and whole genomes of Whitely's specimens from Peru ($n = 4$), from which we obtained diagnostic DNA sequence fragments. We discovered that the putative type series for the taxon *peruviana* includes both giant hummingbird species: one southern and three northern giant hummingbirds. Compounding this error, there are conflicting historical accounts regarding the definition and diagnosis of *peruviana* (*SI Appendix*, Table S5), and the world's major museum collections identify *P. gigas* from Peru as *peruviana* despite their specimen series containing a mix of northern and southern species. Because of the mixed type series, lack of diagnostic characteristics, and historic, ongoing misapplication of its name to both species, the name *peruviana* is *nomen dubium* and should be considered invalid (57).

Our migration-tracking, genomic, physiological, and morphological analyses reveal that the northern, high-elevation resident giant hummingbird populations comprise a new species, which we describe here:

***Patagona chaski* sp. nov.**
Northern Giant Hummingbird
Picaflor gigante del norte (Spanish)

Holotype. CORBIDI AV-012403, MSB:Bird:33080; PERU: dept. Cusco, Prov. Urubamba, district Ollantaytambo, loc. Choquechaca, 13°11.620′S, 72°13.972′W, elev. 4,030 m, 8 March 2009. Male. Parts saved: skin, blood, heart, muscle, liver, lung, pancreas. Prepared by Emil Bautista; personal catalog number EBO 1108. Specimen record: https://arctos.database.museum/guid/MSB:Bird:33080.

Generic placement. The new species is placed unambiguously in the genus *Patagona* Gray 1840, sister to *P. gigas*. It shares the diagnostic traits of *Patagona* described in Elliot (1879:67) (58).

Species diagnosis. Nuclear and mitochondrial DNA indicate ancient (~2.1 to 3.4 Mya) divergence from the southern giant hummingbird, *P. gigas*. The two species are distinguished by substantial differences in migratory behavior and nuclear and mitochondrial genomes and subtle differences in external measurements, plumage coloration, and respiratory traits (Figs. 1–4). Adult northern giant hummingbirds typically have whitish throats with dark streaks, a subtle cinnamon patch at the base of the throat, and a whitish eye-ring with postocular spot.

Comparisons with similar taxa. The southern giant hummingbird has a warm brown to cinnamon throat with subtly contrasting brown streaks, occasionally with a subtle cinnamon patch at the base. Its eye-ring and postocular spot are typically buffy-colored and reduced in extent, giving its face a "blank" appearance.

Paratypes. MSB:Bird catalog numbers: 27069, 27073, 27221, 27222, 31526, 31535, 31536, 31544, 28417, 31666, 28425, 28428, 28472, 31701, 31707, 31714, 31719, 33044, 33293, 34869, 34883, 35069, 36024, 36053, 43771, 43774, 57466, 57480, 57492, 57493, 57496, 57497, 57501, 57502, 57506, 57508, and 57509.

Description of paratypes. We designate 37 adult *P. chaski* paratypes (23 females, 14 males), definitively identified by DNA sequence data or unambiguous consilience of plumage patterns with breeding-season locality. Paratypes were collected from 2006 to 2022 from Ancash, Cusco, Lima, and Tacna departments of Peru. Together, the paratypes approximate the range of plumage variation that we have observed in *P. chaski*.

Specimens examined. A total of 375 *Patagona* specimens were examined and measured from collections in the United States, United Kingdom, and Peru, including 193 specimens of *P. chaski*, 155 specimens of *P. gigas*, 1 hybrid *P. chaski* × *P. gigas*, and 26 specimens of unknown lineage.

Distribution and habitat. *P. chaski* is found in arid and semiarid habitats on the west slope of the Andes and in intermontane valleys, including montane scrub, hedgerows, agricultural areas, open woods (including *Polylepis*), and gardens, often with *Agave*, *Puya*, and *Cactaceae* spp. Across its range, it tends to associate with fast-flowing streams. It spans an elevational range of ~1,800 to 3,600 m in Ecuador, ~1,900 to 4,300 in Peru, and ~1,900 to 3,800 m in Chile.

Etymology. The species name *chaski* is Quechua for "messenger", referring to the revered relay runners who transported messages and goods throughout the Inka Empire (59). At its peak in the late 15th century, the Inka Empire encompassed the entirety of the northern giant hummingbird range. Chaski runners were sure-footed sprinters, capable of speed and endurance on steep slopes, in part due to high-capacity lungs and rigorous aerobic training at high elevations. In addition to speed, chaskis were known for their ability to memorize, transport, and recite important messages. The northern giant hummingbird is the dominant avian pollinator species across much of the former Inka territory, and it has a well-honed spatial memory, and extraordinary aerobic capacity and agility; it thus embodies a closely analogous suite of characteristics.

Nomenclature. *Patagona chaski* was registered on ZooBank and received the following LSID: urn:lsid:zoobank.org:pub:D2D498B7-1427-4A56-81F9-BFEA8C9CB6F5.

Conclusions

The exceptionally broad climatic niche encompassed by the giant hummingbird was illusory, because it represented the combined niches of two cryptic species. During the late Pliocene, giant hummingbirds underwent a striking shift in migratory behavior that was associated with climatic niche breadth expansion. Migratory and sedentary giant hummingbird populations breeding in drastically different elevational environments then underwent speciation with subdivision of the niche. Speciation was likely driven by a combination of geography and diversifying selection caused by breeding range environmental differences and the physiological challenges of extreme migration. The southern giant hummingbirds undertake an extraordinary migratory journey, a loop route that comprises the longest-distance hummingbird migration with the greatest elevational change. Elevational migration evolved in southern giant hummingbirds with a tempo of ascent that facilitates acclimatization. Giant hummingbirds that shift elevations seasonally differ from residents in lung and blood traits, consistent with performance trade-offs. The northern form is the largest hummingbird in the world, a new species that we name *P. chaski*. We suggest the English name northern giant hummingbird and the Spanish name picaflor gigante del norte. That such a conspicuous and charismatic species has remained hidden in plain sight for hundreds of years underscores the power of evolution to maintain phenotypic stasis,

even after migration and climatic niches diverged, spurring genetic and respiratory trait differences and speciation.

Materials and Methods

Sampling. We collected data from 375 wild-caught and specimen-vouchered giant hummingbirds from Ecuador, Peru, Bolivia, Argentina, and Chile (*SI Appendix*, Fig. S2). We weighed each individual (in grams) and measured morphological characteristics (length of bill, total head, wing chord, tail, and tarsus; all in millimeters). Data were obtained from museum specimens collected from 1868 to 2022 from the Museum of Southwestern Biology (MSB), American Museum of Natural History, Harvard Museum of Comparative Zoology, and Cornell University Museum of Vertebrates, and Centro de Ornitología y Biodiversidad (CORBIDI; *SI Appendix*).

Tracking Hummingbird Migration. We affixed 57 geolocator or satellite transmitter tracking devices to giant hummingbirds breeding at low elevation in Valparaíso Region, Chile from 2017 to 2019 (*SI Appendix*, Fig. S1*D*). Devices were attached using the customizable backpack harness and method described in ref. 23. We retrieved 7 of 47 possible geolocators (six devices after 1 y and one device after 2 y) (23) (*SI Appendix*, Table S6).

Migration Analysis. We verified twilights and screened for outliers with the R package TwGeos (https://github.com/slisovski/TwGeos; *SI Appendix*; *SI Appendix*, Fig. S13). We estimated migration tracks in the R package FLightR v0.5.2 (60), following recommendations (61–63). Calibration periods were selected based on periods when each tag was in a known location at the deployment site. We refined our analysis to the giant hummingbird's range by creating a custom land mask (*SI Appendix*). We ran final models with 10e6 particles and check.outliers=TRUE, visualizing estimate error using the *plot_lon_lat* function (*SI Appendix*, Fig. S14). We calculated summary statistics and likely stationary periods using *stationary.migration.summary* and estimated arrival dates to the breeding area with *find.times.distribution* (*SI Appendix*, Table S1). Stationary periods and median tag locations from the location posterior distributions were used to estimate migration tracks. Final tracks excluded 2-wk periods surrounding spring and fall equinoxes (March 17 to 23 and September 15 to 29), respectively. We used the *elevation* function in the package rgbif 3.7.7 (64) to estimate the minimum and maximum seasonal elevations of each tracked giant hummingbird; from these, we calculated total magnitudes of seasonal elevational transition (*SI Appendix*, Table S1).

Our platform terminal transmitter (PTT) satellite devices obtained 1,324 location fixes (PTT 177846 = 847 fixes and PTT 177845 = 477 fixes). PTT 177845 transmitted from 02 February 2019 to 23 February 2019 and PTT 177846 transmitted from 01 February 2019 to 19 July 2020. We applied the Douglas Argos-filter (DAF) algorithm via MoveBank (65), using the "best hybrid" method and following recommended protocols (65) (*SI Appendix*). We used the *elevation* function in rgbif to retrieve elevations from all Argos coordinates, and we removed any observation whose retrieved elevation differed from estimated Argos elevation by ≥300 m, suggestive of error. We excluded from final analysis any observations with <3 messages from Argos satellites (i.e., all observations of location class B). After filtering, PTT 177846 provided 286 high-quality fixes and 164.43 d of transmission data (*SI Appendix*). We did not analyze data from PTT 177845 due to device and/or transmission failure after 20.3 d (*SI Appendix*). We analyzed rates of elevational ascent by calculating meters per day elevation change during the first 21 d of ascent (period from 12 February 2019 to 05 March 2019; Fig. 1 *C* and *E* and *SI Appendix*, Fig. S3).

Blood Data Collection. We sampled blood data from 175 individuals from Peru and Chile from 2006 to 2022 following procedures described in ref. 50. We collected blood from tracked birds by clipping a toenail and blotting <10 μL blood onto a Whatman FTA card and from collected birds by obtaining whole blood within ~5 min to ~3 h of capture by brachial venipuncture and collection with heparinized microcapillary tubes and Hemocue HB201+ cuvettes. Hct (%) was measured with digital calipers after centrifuging the sealed microcapillary tube for 5 min at 13,000 r.p.m. When >1 Hct sample was taken, weighted averages were used. Hemoglobin concentration ([Hb] (g/dL blood) was measured on ~5 μL of blood using a HemoCue HB201+ hemoglobin photometer, with a correction for avian blood (66). We sampled 10 μL whole blood diluted in 1:200 in NaCl solution; we then pipetted a subsample of the dilution into a hemocytometer, allowing cells to settle for 1 min, before photographing at 100× magnification. We estimated TRBC (67, 68) by counting cells in ImageJ (69). After blood sampling, birds were humanely killed and prepared as study skins. Specimens and tissues are housed at the MSB at the University of New Mexico, CORBIDI, and Pontificia Universidad Católica de Chile. Secondary blood indices (MCV, MCH, and MCHC) were calculated from primary indices following standard protocols (67).

Blood Data Analysis. We assessed differences in six blood traits ([Hb], Hct, TRBC, MCV, MCH, and MCHC) using one-way ANOVAs with Tukey's post hoc tests or Kruskal–Wallis tests with Dunn post hoc tests. We did this for three populations of giant hummingbirds: 1) Southern giant hummingbirds sampled at low elevations in Chile during the breeding season; 2) Southern giant hummingbirds sampled at high elevations in Peru during the nonbreeding season (elevational migrants); and 3) Northern high-elevation residents sampled from Peru (Fig. 4 and *SI Appendix*, Table S7). All available data were used for each trait comparison. Exact sample sizes differed for each compared blood trait. Additional details are described in *SI Appendix*.

DNA Extraction and Sequencing. DNA was extracted from frozen muscle tissue, blood preserved on Whatman FTA cards, and toe pad samples from historic museum specimens (*SI Appendix*). We used Sanger sequencing of the mitochondrial gene NADH dehydrogenase subunit II (*ND2*) and exons 1 to 2 of the β^A-globin subunit of hemoglobin, conducted at the UNM Molecular Biology Core Facility. Whole-genome library preparation was performed by the University of Oregon Genomics and Cell Characterization Core Facility (GC3F). Pooled libraries for 36 giant hummingbirds were sequenced for 150 bp PE reads on a full NovaSeq 6000 S4 lane. Library preparation, enrichment of UCEs, and Illumina sequencing were performed by Rapid Genomics (Gainesville, FL) for enrichment of 5,060 UCE loci (Tetrapod UCE 5K probe set) (70) using proprietary chemistry and workflows. Target capture samples were pooled equimolar within shearing groups and sequenced for PE 150 reads on an full Illumina HiSeq 3000 lane. Resequencing of eight whole toe pad genomes was additionally performed by Rapid Genomics. See *SI Appendix* for additional details about DNA extraction, library preparation, and sequencing.

Sequence Data Filtering and Variant Calling. We performed sequence trimming, adapter removal, and quality filtering with Trimmomatic (71) on demultiplexed reads from whole genomes of 36 giant hummingbirds. Cleaned reads were aligned to the annotated Anna's hummingbird (*Calypte anna*) reference genome (GenBank Accession GCA_003957555.2) using BWA-*mem* v0.7.17 (72). We used the Genome Analysis Toolkit (GATK) v4.1.9 tool MarkDuplicatesSpark (as in ref. 73) to mark PCR duplicates and sort BAM files. We genotyped samples using GATK v3.8 UnifiedGenotyper (74) and used GATK3 RealignerTargetCreator and IndelRealigner to call and realign insertions/deletions. All steps were parallelized per individual or using a scatter-gather approach with GNU Parallel 20210922 (75). From genotyped variants, we used GATK4 and VCFtools v0.1.16 (76) to filter variant calls for missing data, coverage, and quality. In GATK4, we used the following variant removal parameters: DP < 4, QUAL < 30, QD < 2, FS > 60.0, and MQ < 40.0. We retained only biallelic variants with minor allele counts ≥2 [i.e., no singletons (77)] and removed sites with minimum mean depth values ≥6. We generated 75% (100,238 SNPs), 95% (100,217 SNPs), and 100% (100,179 SNPs) complete matrices, each with a thinning parameter of 10,000 (i.e., sampling one in every 10,000 base pairs) and that excluded the *W*-chromosome, from 43,566,286 total SNPs.

We processed UCE data following the phyluce v1.7.1x (Faircloth, 2016; https://github.com/faircloth-lab/phyluce) (78) and seqcap_pop pipelines (https://github.com/mgharvey/seqcap_pop) (79). We assembled UCE reference contigs in SPAdes v3.15.3 (80) from sample LSUMNS B7901. Adaptor sequences and low-quality bases were removed with illumiprocessor v2.10, following recommendations. We used phyluce to map contigs to probes and followed the BWA-*mem* and GATK pipeline steps described above but marked duplicates with Picard v2.26.10 MarkDuplicates. In GATK4, we removed variants with the following parameters: QUAL < 30, FS > 60.0, and MQ < 40.0. We used VCFtools to generate a 100% complete dataset (10,000 thinning) with one SNP per locus for UCEs from tissue samples ($n = 35$), which was used to produce a PCA of 4,126 SNPs (*SI Appendix*, Fig. S4*B*) and in downstream analyses. We used the same VCFtools filtering parameters to calculate heterozygosity from tissue UCE data, generating a 100% complete .het file with 10,000 thinning.

We followed the phyluce pipeline to assemble UCE contigs from cleaned reads with SPAdes v3.15.3 (80) and extracted contigs for each taxon that matched UCE loci. We processed only those UCEs derived from tissue samples of *P. gigas*

individuals. We harvested UCE loci from three reference genomes to use as outgroups: *C. anna*, black-breasted hillstar (*Oreotrochilus melanogaster*; GenBank BioSample SAMN12253978) (81) and long-tailed hermit (*Phaethornis superciliosus;* GenBank Accession PRJNA789234) (82). We aligned UCE loci using mafft v7.490 (83) with edge and internal trimming, and used Gblocks v0.91 (84) to clean trimmed alignments. We generated a 100% complete matrix containing data from five individuals (one northern and one southern *Patagona* plus outgroups; 4,285 alignments) for downstream analysis. In all analyses involving genomes and UCEs (and all VCF files produced from these data), we removed a single Chilean individual (MSB:Bird:56153) that was found to be related to MSB:Bird:56167.

Using a variant of the seqcap_pop pipeline described above, we aligned whole-genome data to our UCE reference to obtain homologous SNPs from both datasets for population structure analyses. We used a custom pipeline and Python scripts (85) to combine these two data types. In brief, we separated whole-genome and target capture UCEs and, for each dataset, removed loci above a threshold of cross-lineage heterozygosity ($H_O = 0.4$) to account for misaligned reads and paralogs, after which we merged datasets in VCFtools. After applying the heterozygosity filter, we combined the two datasets and generated a 90% complete dataset and one SNP per locus for $n = 70$ individuals. UCE data from toe pads of historic specimens ($n = 30$ individuals) were highly degraded and were analyzed separately from tissue data (*SI Appendix*).

Population Assignment and Structure Inference. We used multiple approaches to determine population structure within *Patagona*. First, we conducted PCAs of SNPs with all UCE data ($n = 70$ individuals; 4,416 SNPs; 90% complete dataset), whole-genome data ($n = 35$ individuals; 100,238 SNPs; 75% complete dataset), and separately for tissue UCE data ($n = 35$ individuals; 4,126 SNPs; 100% complete matrix; *SI Appendix*). Results were concordant across datasets (Fig. 2 and *SI Appendix*, Fig. S4). Second, we estimated individual ancestry coefficients using model-based clustering sparse nonnegative matrix factorization (NMF) with snmf in LEA 3.10.2 (86) using a 100% complete input whole-genome dataset ($n = 35$ individuals, 100,179 SNPs). Analyses were performed for $K = 1$ to 4 (Fig. 2*D*) with a range of alpha (α) regularization parameter values and 100 repetitions for each K value (*SI Appendix*). Values of *K* were selected based on *a priori* hypotheses about resident–migrant divergence and range-wide population structure. We present admixture results from the estimated best-fit *K*, determined by the lowest cross-entropy criterion values at $\alpha = 100$. Finally, we used *ND2* sequences to generate a minimum-spanning haplotype network (87) in PopART (88) (Fig. 2*E*). Individuals without genetic data were carefully classified to lineage, typically using multiple methods (*SI Appendix*, Table S8).

Demographic Modeling. We prepared PSMC input files by creating a consensus diploid sequence for each sample (i.e., a single representative individual from each country-level population with >18× coverage) using a pipeline combining SAMtools v1.14 (89), Picard v2.26.10, and BCFtools v1.14. We used the *C. anna* genome as a reference. We converted the consensus VCF to fastq format using the vcf2fq command of the vcfutils script in SAMtools, removing bases with quality < 30 (−Q), a minimum read depth of 10 (−d), and a maximum read depth of 50 (−D). The consensus fastq sequence was converted to PSMC input format using the PSMC fq2psmcfa script (34).

DNA from Historic Toe Pad Samples. We obtained UCEs from toe pads of historic specimens ($n = 30$ individuals) and whole genomes from $n = 8$ toepad samples. We used fragments of the mitogenome to definitively place four Bolivia samples and four Whitely specimens ($n = 2$ from Tinta, Cusco, Peru; $n = 2$ from Cachupata, Cusco, Peru) to lineage of origin (*SI Appendix*, Fig. S15).

Mitogenomes and Mitochondrial Sequence Data. We used the BCFtools consensus sequence pipeline described for PSMC input to obtain whole mitogenomes and the mitochondrial *ND2* gene from genomic sequence data (*SI Appendix*). We used a mitogenome from the versicolored emerald (*Amazilia versicolor*; [(90)] (GenBank Accession NC_024156) to obtain a reference mitogenome of *P. gigas* (MSB:Bird:28366; 27.08× coverage), which we then used to obtain mitogenomes from both whole genomes ($n = 35$) and historic toe pad samples ($n = 8$). We obtained *ND2* sequences by mapping whole-genome and UCE data separately to a *P. gigas* reference sequence (LSUMNS B6303; GenBank Accession AY830510.1). All mitochondrial sequences were checked and aligned in Geneious Prime 2022.2.2 (91).

Phylogenetic Inference and Divergence Time Estimation. We estimated divergence times and phylogenetic relationships with nuclear (UCE) and mitochondrial (*ND2*) DNA. Our *ND2* dataset included 100% complete sequence data (1,041 bp) from one representative northern (LSUMNS B7901) and southern (MSB:Bird:56142) giant hummingbird plus six outgroups, representing seven of the nine hummingbird clades (*SI Appendix*). *ND2* phylogenies were estimated using maximum likelihood (ML) in RAxML v8.2.4 (92) and Markov chain Monte Carlo (MCMC) in Beast2 2.6.7 (93) (*SI Appendix*, Fig. S5). In RAxML, we used the GTR+G model of nucleotide substitution and conducted bootstrap analysis with 1,000 replicates, after which we searched for the best scoring ML tree. In Beast2, we used the HKY+I+G model of nucleotide substitution with gamma category count of 4, a relaxed log normal clock model, and a Yule speciation tree prior. Our UCE phylogeny was estimated from a 100% complete concatenated dataset with five individuals: one northern (MSB:Bird:33353) and one southern (MSB:Bird:34857) *Patagona*, plus three outgroups (*P. superciliosus*, *O. melanogaster*, and *C. anna*). We generated 10 subsets of 100 UCE loci chosen at random. In Beast2 (version 2.6.3), we used the HKY+I+G model of nucleotide substitution with gamma category count of 4, a relaxed log normal clock model, and a Birth Death speciation tree prior.

For nuclear and mitochondrial Beast analyses, we applied two secondary calibrations from ref. 18: 1) A crown age prior (normal distribution; monophyletic; mean = 22.46, sigma = 1.12); and 2) A prior capturing the split between *Patagona* and the Emerald, Bee, and Mountain-gem clades (normal distribution; monophyletic; mean = 14.4, sigma = 0.7). We ran the *ND2* tree for 20 million generations, sampling every 2,000 steps, and the UCE tree for 100 million generations, sampling every 10,000 steps. Fits were assessed using Tracer v1.7.2 (http://tree.bio.ed.ac.uk/software/tracer; *SI Appendix*). We conducted two independent runs for the *ND2* tree (2 runs total) and two independent runs of each subset for the UCE tree (20 runs total). We summarized maximum clade credibility trees using LogCombiner and TreeAnnotator, discarding the first 10% of MCMC generations as burn-in (94).

Tests of Gene Flow. We tested for gene flow between northern and southern lineages using ABBA/BABA tests implemented in Dsuite 0.4r38 (95) (https://github.com/millanek/Dsuite). Each input VCF for ABBA/BABA tests included 15 whole genomes (the three highest-coverage genomes from each Ecuador and Peru (representing northern birds) and from each Chile and Argentina (representing southern birds), plus three *A. alexandri* outgroups (Sequence Read Archive accessions: SRR12247328, SRR12247329, and SRR12247340) (18). This enabled us to compare all viable introgression scenarios among countries. For each ABBA/BABA test, we calculated Patterson's *D* and f_4-ratios of admixture proportion (96, 97) and estimated significance using jackknifing. We used several input datasets for ABBA/BABA tests, including 100% and 95% complete VCFs with and without the Z-chromosome. Results were consistent when comparing different input datasets. We report the results of our 100% complete dataset without the *W* and *Z* chromosomes in *SI Appendix*, Table S2.

Population Divergence and Nucleotide Diversity. We assessed the levels of divergence and nucleotide diversity across the genome by calculating F_{ST}, π, and Tajima's *D*. We estimated Weir and Cockerham's genome-wide weighted F_{ST} (98) in 10 and 50 kilobase (kb) windows for all lineage-level and country-level pairwise comparisons using VCFtools 0.1.6. We repeated comparisons for autosomal data (excluding *Z* and *W*-chromosomes) and separately for the *Z*-chromosome. For F_{ST} calculations, we visualized the results and produced Manhattan plots using the R package qqman v0.1.8 (99). For calculation of mean genome-wide $F_{ST,}$ we used the 75% complete dataset with 10,000 thinning.

Tajima's *D* input files were created in VCFtools 0.1.6, using an input VCF of invariant sites (i.e., no variant or indel selection and filtration) but with the EMIT_ALL_SITES output mode of UnifiedGenotyper and without GATK filtering. In VCFtools, we excluded the *Z*- and *W*-chromosomes and filtered by max-alleles = 2 and min-mean DP = 4. After filtering, we kept 907,893,210 out of 1,043,590,471 possible sites. Our output VCF file was 75% complete with thinning every 10,000 steps. We then used pixy v1.6.2.beta1 to estimate population-level (i.e., Ecuador, Peru, Argentina, and Chile) nucleotide diversity (π) and Tajima's *D* over a 10-kb window size. We estimated per-population mean nucleotide diversity to prevent overinflation of per-lineage (northern and southern) nucleotide diversity due to population structure within lineages. Instead, we calculated per-lineage nucleotide diversity

using per-population estimates of π: Southern π was calculated as mean(Argentina π, Chile π) and northern π was calculated as mean(Ecuador π, Peru π).

Morphological Analysis. We analyzed mensural and relative organ mass differences between northern and southern forms (Fig. 4), and between males and females of northern and southern forms (*SI Appendix*, Fig. S7), using t-tests and nonparametric Wilcoxon rank-sum tests. We characterized morphological variation in bill length, wing length, and tail length between species and separately for males and females using PCA in ggfortify v0.4.1. We conducted Linear Discriminant Analysis (LDA) of bill, wing, and tail measurements using the R package MASS 7.3.58.3 (100) separately for males and females. Models correctly classified females to lineage in 64.5 to 82.8% of cases and males correctly in 79.5 to 85.7% of cases, depending on the model (*SI Appendix*, Fig. S8); however, there was substantial overlap in individual morphological characteristics. All available data were used for each trait comparison. Exact sample sizes differed for each compared trait (*SI Appendix*).

Ethics and Inclusion Statement. This study was a collaborative effort among the Museum of Southwestern Biology at the University of New Mexico in the United States, the Centro de Ornitología y Biodiversidad in Peru, and Pontificia Universidad Católica de Chile in Chile. Authors from all institutions and from the United States, Peru, and Chile are included. Biological samples and vouchered specimens are deposited at all three institutions and their data are openly accessible in public databases for reproducibility and extension.

Data, Materials, and Software Availability. Specimen data are available in the ARCTOS database (www.arctosdb.org) (101). Fastq files for genomes and UCEs have been deposited on the Sequence Read Archive (BioProject PRJNA1101054) (102); migration tracks on MoveBank (www.movebank.org (103); Project ID: 3594892529 (104)); and analysis scripts and code on GitHub (https://github.com/jlwilliamson/patagona-blood-migration-genomics (105); https://doi.org/10.5281/zenodo.10975589 (106)). Raw data have been deposited on Dryad (https://doi.org/10.5061/dryad.44j0zpcnp) (107).

ACKNOWLEDGMENTS. We dedicate this paper to our inimitable coauthor and friend, Pancho Bozinovic, who passed away before this work was completed. We thank Mark Adams, Mike Andersen, Lisa Barrow, John Bates, Carla Bautista, Evelin Bautista, Nahisa Bautista, Yoselin Bautista, Dulia Bautista, Phred Benham, David Benvent, Bentley Bird, Sharon Birks, Jeff Bishop, Jose Miguel Bogdanovich, Mariel Campbell, Malé Castro Farías, Marlon Chagua, Andrea Chavez, Jocie Colella, Eamon Corbett, Joel Cracraft, Charles Dardia, Jillian Ditner, Jonathan Duran, Scott Edwards, Annette Estevez, Rob Faucett, Cristhian Felix, Monica Flores, Will Ford, Mary Margaret Ferraro, James Fox, John Gerwin, Avia González-Mendez, Gary Graves, Chuck Hathcock, Andy Johnson, John Klicka, Gunnar Kramer, Andy Kratter, Ethan Linck, Schuyler Liphardt, Manuela Londoño, Terry Lott, LyAndra Lujan, Ben Marks, Alan Marsh, Kevin McCracken, Chris Milensky, Kyana Montoya, Rob Moyle, Paloma Ordoñez, Jose Antonio Otero, Eldar Rakhimberdiev, Javier Reinoso, Mark Robbins, Bryce Robinson, Vanya Rohwer, George Rosenberg, Benito Rosende, Jennifer Rudgers, Frank Solano Bravo, Dave Steadman, Eli Stone, Henry Streby, Paul Sweet, Jeremiah Trimble, Tom Trombone, Hein van Grouw, J. V. Remsen, Jr., Yessenia Velasquez Taramona, Jen Walsh, and Ariel Woodward. We are grateful for detailed constructive feedback from three anonymous reviewers and our editor. We thank the communities of Acquia, Candarave, Chuquibamba, Lucre, Macate, Ocros, Oncoy, Ollantaytambo, Pacaraos, Pueblo Libre, San Antonio de Cusicancha, San Marcos, San Pedro de Casta, Santiago de Carampoma, and Urubamba for site access in Peru, and Margarita Espinoza and Alfredo Zelada for site access in Chile. Tissue loans and collections access were provided by the Museum of Southwestern Biology, American Museum of Natural History, Smithsonian National Museum of Natural History, Cornell University Museum of Vertebrates, The Burke Museum at the University of Washington, University of Kansas Biodiversity Institute, Florida Museum of Natural History, Louisiana State University Museum of Natural Science, Harvard Museum of Comparative Zoology, and Centro de Ornitología y Biodiversidad. Sequencing and bioinformatics were facilitated by the Center for Advanced Research Computing and Molecular Biology Core Facility at the University of New Mexico, the University of Oregon Genomics and Cell Characterization Core Facility, and Rapid Genomics. This work was supported by Dr. Mike Hartshorne and Dr. Lida Crooks, NSF (DEB-1146491, DBI-2208924), a Cornell Lab of Ornithology Edward W. Rose Postdoctoral Fellowship, and grants to JLW from the American Philosophical Society, Explorers Club, Society of Systematic Biologists, American Ornithological Society, Wilson Ornithological Society, Nuttall Ornithological Club, American Museum of Natural History (Frank M. Chapman Memorial Fund), UNM Biology Graduate Student Association Graduate Research Allocations Committee, University of New Mexico Graduate and Professional Student Association, University of New Mexico Latin American & Iberian Institute, and University of New Mexico Department of Biology Grove, Melinda Bealmear, and Dr. Jones & Dr. Wong Research Scholarships. Permits in Chile were granted by Servicio Agrícola y Ganadero (Resolución Exenta Nos.: 7593/2016, 6817/2017, 7903/2018, 6691/2018, 6692/2018, 6693/2018, and 6694/2018). Permits in Peru were granted by Servicio Nacional Forestal y de Fauna Silvestre (Resolución Directoral Nos.: 004-2007-INRENA-IFFS-DCB, 135-2009-AG-DGFFS-DGEFFS, 0377-2010-AG-DGFFS-DGEFFS, 0199-2012-AG-DGFFS-DGEFFS, and 006-2013-MINAGRI-DGFFS/DGEFFS, 244-2020-MINAGRI-SERFOR/DGGSPFFS-DGSPFS). University of New Mexico Institutional Animal Care and Use Committee approval was granted under protocols 16-200596-MC, 19-200967-MC, and 16-200418-MC.

Author affiliations: [a]Museum of Southwestern Biology, University of New Mexico, Albuquerque, NM 87131; [b]Department of Biology, University of New Mexico, Albuquerque, NM 87131; [c]Cornell Lab of Ornithology, Cornell University, Ithaca, NY 14850; [d]Department of Ecology and Evolutionary Biology, Cornell University, Ithaca, NY 14850; [e]Centro de Ornitología y Biodiversidad, Lima 15064, Peru; [f]Environmental Stewardship, Los Alamos National Laboratory, Los Alamos, NM 87545; [g]The Earth Commons Institute, Department of Biology, McCourt School of Public Policy, Georgetown University, Washington, DC 20057; [h]Facultad de Artes Liberales, Departamento de Ciencias, Universidad Adolfo Ibáñez, Santiago 7941169, Chile; [i]Facultad de Ciencias Forestales, Universidad Nacional Agraria La Molina, Lima 15024, Peru; [j]Departamento de Ecología, Center of Applied Ecology and Sustainability, Facultad de Ciencias Biológicas, Pontificia Universidad Católica de Chile, Santiago 3542000, Chile; and [k]Department of Biology, Institute of Ecology and Evolution, University of Oregon, Eugene, OR 97403

1. R. MacArthur, *Geographical Ecology: Patterns in the Distribution of Species* (Princeton University Press, 1972).
2. J. T. Anderson, C. R. Lee, C. A. Rushworth, R. I. Colautti, T. Mitchell-Olds, Genetic trade-offs and conditional neutrality contribute to local adaptation. *Mol. Ecol.* **22**, 699–708 (2013).
3. L. M. Bono, L. B. Smith, D. W. Pfennig, C. L. Burch, The emergence of performance trade-offs during local adaptation: Insights from experimental evolution. *Mol. Ecol.* **26**, 1720–1733 (2017).
4. M. C. Whitlock, The red queen beats the jack-of-all-trades: The limitations on the evolution of phenotypic plasticity and niche breadth. *Am. Nat.* **148**, S65–S77 (1996).
5. J. P. Sexton, J. Montiel, J. E. Shay, M. R. Stephens, R. A. Slatyer, Evolution of ecological niche breadth. *Annu. Rev. Ecol. Evol. Syst.* **48**, 183–206 (2017).
6. K. A. Carscadden *et al.*, Niche breadth: Causes and consequences for ecology, evolution, and conservation. *Q. Rev. Biol.* **95**, 179–214 (2020).
7. J. Grinnell, Barriers to distribution as regards birds and mammals. *Am. Nat.* **48**, 248–254 (1914).
8. M. Ackermann, M. Doebeli, Evolution of niche width and adaptive diversification. *Evolution (N. Y).* **58**, 2599–2612 (2004).
9. D. J. Futuyma, G. Moreno, The evolution of ecological specialization. *Annu. Rev. Ecol. Syst.* **19**, 207–233 (1988).
10. N. Janz, S. Nylin, "The oscillation hypothesis of host-plant range and speciation" in *Specialization, Speciation, and Radiation: The Evolutionary Biology of Herbivorous Insects*, K. J. Tilmon, Ed. (University of California Press, 2008), pp. 203–215.
11. C. Gómez-Rodríguez, A. Baselga, J. J. Wiens, Is diversification rate related to climatic niche width? *Glob. Ecol. Biogeogr.* **24**, 383–395 (2015).
12. N. B. Hardy, S. P. Otto, Specialization and generalization in the diversification of phytophagous insects: Tests of the musical chairs and oscillation hypotheses. *Proc. R. Soc. B Biol. Sci.* **281**, 20132960 (2014).
13. E. H. Day, X. Hua, L. Bromham, Is specialization an evolutionary dead end? Testing for differences in speciation, extinction and trait transition rates across diverse phylogenies of specialists and generalists. *J. Evol. Biol.* **29**, 1257–1267 (2016).
14. V. Gómez-Bahamón *et al.*, Speciation associated with shifts in migratory behavior in an avian radiation. *Curr. Biol.* **30**, 1–10 (2020).
15. B. Kondo, J. L. Peters, B. B. Rosensteel, K. E. Omland, Coalescent analyses of multiple loci support a new route to speciation in birds. *Evolution (N. Y).* **62**, 1182–1191 (2008).
16. J. I. Areta *et al.*, Rapid adjustments of migration and life history in hemisphere-switching cliff swallows. *Curr. Biol.* **31**, 2914–2919.e2 (2021).
17. J. Rolland, F. Jiguet, K. A. Jønsson, F. L. Condamine, H. Morlon, Settling down of seasonal migrants promotes bird diversification. *Proc. R. Soc. B Biol. Sci.* **281**, 20140473 (2014).
18. J. A. McGuire *et al.*, Molecular phylogenetics and the diversification of hummingbirds. *Curr. Biol.* **24**, 1–7 (2014).
19. D. A. Skandalis *et al.*, The biomechanical origin of extreme wing allometry in hummingbirds. *Nat. Commun.* **8**, 1–9 (2017).
20. M. J. Fernández, R. Dudley, F. Bozinovic, Comparative energetics of the giant hummingbird (*Patagona gigas*). *Physiol. Biochem. Zool.* **84**, 333–340 (2011).
21. C. Darwin, "'Trochilus gigas'" in *The Zoology of the Voyage of the H.M.S. Beagle* (Smith, Elder, and Co., 1839).

22. C. H. Hellmayr, *The Birds of Chile* (Field Museum Press, Chicago, IL, USA, 1932).
23. J. L. Williamson, C. C. Witt, A lightweight backpack harness for tracking hummingbirds. *J. Avian Biol.* **52**, 1–9 (2021).
24. S. R. Supp *et al.*, Citizen-science data provides new insight into annual and seasonal variation in migration patterns. *Ecosphere* **6**, 1–19 (2015).
25. C. T. Sahley, Bat and hummingbird pollination of an autotetraploid columnar cactus, *Weberbauerocereus weberbaueri* (Cactaceae). *Am. J. Bot.* **83**, 1329–1336 (1996).
26. F. Johow, Las cactacea de los alrededores de Zapallar. *Rev. Chil. Hist. Nat.* **15**, 152–166 (1921).
27. H. Walter, Floral biology, phytogeography and systematics of Eriosyce subgenus Neoporteria (Cactaceae). *Bradleya* **26**, 75–98 (2008).
28. H. E. Walter, Floral biology of *Echinopsis chiloensis* ssp. chiloensis (Cactaceae): Evidence for a mixed pollination syndrome. *Flora Morphol. Distrib. Funct. Ecol. Plants* **205**, 757–763 (2010).
29. J. L. Williamson, C. C. Witt, Elevational niche-shift migration: Why the degree of elevational change matters for the ecology, evolution, and physiology of migratory birds. *Ornithology* **138**, 1–26 (2021).
30. J. B. West, American medical research expedition to Everest. *High Alt. Med. Biol.* **11**, 103–110 (2010).
31. A. J. Peacock, P. L. Jones, Gas exchange at extreme altitude: Results from the British 40th Anniversary Everest Expedition. *Eur. Respir. J.* **10**, 1439–1444 (1997).
32. S. R. Muza, B. A. Beidleman, C. S. Fulco, Altitude preexposure recommendations for inducing acclimatization. *High Alt. Med. Biol.* **11**, 87–92 (2010).
33. S. M. Billerman, B. K. Keeney, P. G. Rodewald, T. S. Schulenberg, *Birds of the World* (Cornell Lab of Ornithology, 2022).
34. H. Li, R. Durbin, Inference of human population history from individual whole-genome sequences. *Nature* **475**, 493–496 (2011).
35. M. C. Whitlock, D. E. Mccauley, Indirect measures of gene flow and migration: F(ST) ≠ 1/(4Nm + 1). *Heredity (Edinb).* **82**, 117–125 (1999).
36. J. A. Coyne, H. A. Orr, The evolutionary genetics of speciation. *Philos. Trans. R. Soc. B* **353**, 287–305 (1998).
37. E. K. Mikkelsen, D. Irwin, Ongoing production of low-fitness hybrids limits range overlap between divergent cryptic species. *Mol. Ecol.* **30**, 4090–4102 (2021).
38. Y. Licona-Vera, J. F. Ornelas, The conquering of North America: Dated phylogenetic and biogeographic inference of migratory behavior in bee hummingbirds. *BMC Evol. Biol.* **17**, 1–17 (2017).
39. P. Escalante, L. Márquez-Valdelamar, P. De La Torre, J. P. Laclette, J. Klicka, Evolutionary history of a prominent North American warbler clade: The Oporornis–Geothlypis complex. *Mol. Phylogenet. Evol.* **53**, 668–678 (2009).
40. O. Carmi, C. C. Witt, A. Jaramillo, J. P. Dumbacher, Phylogeography of the Vermilion Flycatcher species complex: Multiple speciation events, shifts in migratory behavior, and an apparent extinction of a Galápagos-endemic bird species. *Mol. Phylogenet. Evol.* **102**, 152–173 (2016).
41. T. de Zoeten, F. Pulido, How migratory populations become resident. *Proc. R. Soc. B* **287**, 20193011 (2020).
42. K. M. Gregory-Wodzicki, Uplift history of the Central and Northern Andes: A review. *Geol. Soc. Am. Bull.* **112**, 1091–1105 (2000).
43. R. M. Zink, The evolution of avian migration. *Biol. J.* **104**, 237–250 (2011).
44. C. Sheard *et al.*, Ecological drivers of global gradients in avian dispersal inferred from wing morphology. *Nat. Commun.* **11**, 2463 (2020).
45. R. Lockwood, J. P. Swaddle, J. M. V. Rayner, Avian wingtip shape reconsidered: Wingtip shape indices and morphological adaptations to migration. *J. Avian Biol.* **29**, 273–292 (1998).
46. D. L. Altshuler, Flight performance and competitive displacement of hummingbirds across elevational gradients. *Am. Nat.* **167**, 216–229 (2006).
47. J. Projecto-Garcia *et al.*, Repeated elevational transitions in hemoglobin function during the evolution of Andean hummingbirds. *Proc. Natl. Acad. Sci. U.S.A.* 110, 20669–20674 (2013).
48. Y. Cheng *et al.*, Parallel genomic responses to historical climate change and high elevation in East Asian songbirds. *Proc. Natl. Acad. Sci. U.S.A.* **118**, 1–11 (2021).
49. Y. Qu *et al.*, The evolution of ancestral and species-specific adaptations in snowfinches at the Qinghai–Tibet Plateau. *Proc. Natl. Acad. Sci. U.S.A.* **118**, 1–10 (2021).
50. J. L. Williamson *et al.*, Hummingbird blood traits track oxygen availability across space and time. *Ecol. Lett.* **26**, 1223–1236 (2023).
51. C. Carey, M. L. Morton, Aspects of circulatory physiology of montane and lowland birds. *Comp. Biochem. Physiol. Part A* **54**, 61–74 (1976).
52. C. M. Beall, Andean, Tibetan, and Ethiopian patterns of adaptation to high-altitude hypoxia. *Integr. Comp. Biol.* **46**, 18–24 (2006).
53. M. Kiyamu *et al.*, Developmental and genetic components explain enhanced pulmonary volumes of female Peruvian quechua. *Am. J. Phys. Anthropol.* **148**, 534–542 (2012).
54. L. P. Vieillot, *Colibris et Oiseaux-Mouches* (Chez Desray, A Paris, an XI=1802, 1824).
55. A. Boucard, *Genera of Humming Birds, 21* (London, 1893).
56. E. Simon, Histoire naturelle des trochilidae (Synopsis et catalogue). *Encyclopédie-Roret* **i–vi**, 1–416 (1921).
57. ICZN, *International Code of Zoological Nomenclature* (International Trust for Zoological Nomenclature, ed. 4, 1999).
58. D. G. Elliot, *A Classification and Synopsis of the Trochilidae* (Smithsonian Institution, 1879).
59. F. G. P. de Ayala, *Primer Nueva Corónica y Buen Gobierno* (Hackett Publishing, 1615).
60. E. Rakhimberdiev, A. Saveliev, T. Piersma, J. Karagicheva, FLightR: An R package for reconstructing animal paths from solar geolocation loggers. *Methods Ecol. Evol.* **8**, 1482–1487 (2017).
61. E. Rakhimberdiev *et al.*, Comparing inferences of solar geolocation data against high-precision GPS data: Annual movements of a double-tagged black-tailed godwit. *J. Avian Biol.* **47**, 589–596 (2016).
62. S. Lisovski *et al.*, Light-level geolocator analyses: A user's guide. *J. Anim. Ecol.* **89**, 221–236 (2019).
63. E. Rakhimberdiev *et al.*, A hidden Markov model for reconstructing animal paths from solar geolocation loggers using templates for light intensity. *Mov. Ecol.* **3**, 25 (2015).
64. S. Chamberlain *et al.*, rgbif: Interface to the Global Biodiversity Information Facility API, R package version 1.4.0 (2019).
65. D. C. Douglas *et al.*, Moderating Argos location errors in animal tracking data. *Methods Ecol. Evol.* **3**, 999–1007 (2012).
66. P. Simmons, A. Lill, Development of parameters influencing blood oxygen carrying capacity in the welcome swallow and fairy martin. *Comp. Biochem. Physiol., A Mol. Integr. Physiol.* **143**, 459–468 (2006).
67. T. W. Campbell, C. K. Ellis, *Avian and Exotic Animal Hematology and Cytology* (Blackwell Publishing Professional, 2007).
68. J. Samour, "Diagnostic value of hematology" in *Clinical Avian Medicine, Volume II*, G. Harrison, T. Lightfoot, Eds. (Spix Publishing, Inc. Palm Beach, FL, 2005), pp. 587–610.
69. W. S. Rasband, *ImageJ* (U.S. National Institutes of Health, Bethesda, Maryland, USA, 2018).
70. B. C. Faircloth *et al.*, Ultraconserved elements anchor thousands of genetic markers spanning multiple evolutionary timescales. *Syst. Biol.* **61**, 717–726 (2012).
71. A. M. Bolger, M. Lohse, B. Usadel, Trimmomatic: A flexible trimmer for Illumina sequence data. *Bioinformatics* **30**, 2114–2120 (2014).
72. H. Li, R. Durbin, Fast and accurate short read alignment with Burrows–Wheeler transform. *Bioinformatics* **25**, 1754–1760 (2009).
73. S. Lamichhaney *et al.*, Evolution of Darwin's finches and their beaks revealed by genome sequencing. *Nature* **518**, 371–375 (2015).
74. A. McKenna *et al.*, The Genome Analysis Toolkit: A MapReduce framework for analyzing next-generation DNA sequencing data. *Genome Res.* **20**, 1297–1303 (2010).
75. O. Tange, *GNU Parallel 2021* (2021) https://doi.org/10.5281/zenodo.1146014. Accessed 15 February 2022.
76. P. Danecek *et al.*, The variant call format and VCFtools. *Bioinformatics* **27**, 2156–2158 (2011).
77. E. Linck, C. J. Battey, Minor allele frequency thresholds strongly affect population structure inference with genomic data sets. *Mol. Ecol. Resour.* **19**, 639–647 (2019).
78. B.C. Faircloth, PHYLUCE is a software package for the analysis of conserved genomic loci. *Bioinformatics* **32**, 786–88 (2016).
79. M. G. Harvey, B. T. Smith, T. C. Glenn, B. C. Faircloth, R. T. Brumfield, Sequence capture versus restriction site associated DNA sequencing for shallow systematics. *Syst. Biol.* **65**, 910–924 (2016).
80. A. Bankevich *et al.*, SPAdes: A new genome assembly algorithm and its applications to single-cell sequencing. *J. Comput. Biol.* **19**, 455–477 (2012).
81. S. Feng, Dense sampling of bird diversity increases power of comparative genomics. *Nature* **587**, 252–257 (2020).
82. E. Osipova *et al.*, Loss of a gluconeogenic muscle enzyme contributed to adaptive metabolic traits in hummingbirds. *Science* **190**, 185–190 (2023).
83. K. Katoh, D. M. Standley, MAFFT multiple sequence alignment software version 7: Improvements in performance and usability. *Mol. Biol. Evol.* **30**, 772–780 (2013).
84. J. Castresana, Selection of conserved blocks from multiple alignments for their use in phylogenetic analysis. *Mol. Biol. Evol.* **17**, 540–552 (2000).
85. E. F. Gyllenhaal, X. M. Mapel, A. Naikatini, R. G. Moyle, M. J. Andersen, A test of island biogeographic theory applied to estimates of gene flow in a Fijian bird is largely consistent with neutral expectations. *Mol. Ecol.* **29**, 4059–4073 (2020).
86. E. Frichot, F. Mathieu, T. Trouillon, G. Bouchard, O. François, Fast and efficient estimation of individual ancestry coefficients. *Genetics* **196**, 973–983 (2014).
87. H. J. Bandelt, P. Forster, A. Röhl, Median-joining networks for inferring intraspecific phylogenies. *Mol. Biol. Evol.* **16**, 37–48 (1999).
88. J. W. Leigh, D. Bryant, POPART: Full-feature software for haplotype network construction. *Methods Ecol. Evol.* **6**, 1110–1116 (2015).
89. H. Li *et al.*, The sequence alignment/map format and SAMtools. *Bioinformatics* **25**, 2078–2079 (2009).
90. F. Prosdocimi, H. M. Souto, P. A. Ruschi, C. Furtado, W. B. Jennings, Complete mitochondrial genome of the versicoloured emerald hummingbird *Amazilia versicolor*, a polymorphic species. *Mitochondrial DNA* **27**, 3214–3215 (2016).
91. M. Kearse *et al.*, Geneious basic: An integrated and extendable desktop software platform for the organization and analysis of sequence data. *Bioinformatics* **28**, 1647–1649 (2012).
92. A. Stamatakis, RAxML version 8: A tool for phylogenetic analysis and post-analysis of large phylogenies. *Bioinformatics* **30**, 1312–1313 (2014).
93. R. Bouckaert *et al.*, BEAST 2.5: An advanced software platform for Bayesian evolutionary analysis. *PLoS Comput. Biol.* **15**, 1–28 (2019).
94. A. J. Drummond, M. A. Suchard, D. Xie, A. Rambaut, Bayesian phylogenetics with BEAUti and the BEAST 1.7. *Mol. Biol. Evol.* **29**, 1969–1973 (2012).
95. M. Malinsky, M. Matschiner, H. Svardal, Dsuite–Fast D-statistics and related admixture evidence from VCF files. *Mol. Ecol. Resour.* **21**, 584–595 (2021).
96. E. Y. Durand, N. Patterson, D. Reich, M. Slatkin, Testing for ancient admixture between closely related populations. *Mol. Biol. Evol.* **28**, 2239–2252 (2011).
97. N. Patterson *et al.*, Ancient admixture in human history. *Genetics* **192**, 1065–1093 (2012).
98. B. Weir, C. Clark Cockerham, Estimating F-statistics for the analysis of population structure. *Evolution (N. Y).* **38**, 1358–1370 (2011).
99. S. D. Turner, qqman: An R package for visualizing GWAS results using Q–Q and Manhattan plots. *J. Open Source Software* **3**, 731 (2018).
100. A. Brian, B. Venables, D. M. Bates, D. Firth, M. B. Ripley, *Package 'MASS'* (2022). https://cran.r-project.org/web/packages/MASS/index.html. Accessed 20 May 2022.
101. C. Cicero *et al.*, Arctos: Community-driven innovations for managing biodiversity and cultural collections. In review. biorxiv [Preprint] (2023). https://www.biorxiv.org/content/10.1101/2023.12.15.571899v1 (Accessed 15 April 2024).
102. J. L. Williamson, BioProject PRJNA1101054. Sequence Read Archive. http://www.ncbi.nlm.nih.gov/bioproject/1101054. Accessed 16 April 2024.
103. M. Wikelski, S. C. Davidson, R. Kays, Movebank: archive, analysis and sharing of *animal* movement data. Movebank. https://www.movebank.org/. Accessed 15 April 2024.
104. J. L. Williamson, Project ID: 3594892529. MoveBank. https://www.movebank.org/cms/webapp?gwt_fragment=page=studies,path=study3594892529. Accessed 16 April 2024.
105. J. L. Williamson. jlwilliamson-patagona-blood-migration-genomics. GitHub. https://github.com/jlwilliamson/jlwilliamson-patagona-blood-migration-genomics. Accessed 14 April 2024.
106. J. L. Williamson, jlwilliamson/jlwilliamson-patagona-blood-migration-genomics: giant hummingbirds v2. Zenodo. https://doi.org/10.5281/zenodo.10975589. Accessed 15 April 2024.
107. J. L. Williamson *et al.*, Data from "Extreme elevational migration spurred cryptic speciation in giant hummingbirds" [Dataset]. Dryad. https://doi.org/10.5061/dryad.44j0zpcnp. Deposited 17 April 2024.